Development of an analytical model to predict self-folding of 4D bioprinted scaffolds

Alessio Esposito[1], Irene Chiesa[1], Claudia Dell'Amico[2], Marco Onorati[2], Carmelo De Maria[1]

[1]*Department of Information Engineering and Research Center Enrico Piaggio, University of Pisa, Italy*

[2]*Unit of Cell and Developmental Biology, Department of Biology, University of Pisa, Italy*

***Abstract*—Four Dimensions (4D) printing is a fabrication approach which adds the fourth dimension "time" at the three spatial dimensions of Three-Dimensional (3D) printing. A 4D printed object can change its shape and function after receiving an appropriate stimulus. 4D printing finds application in tissue engineering and biofabrication. Indeed, the change in shape of a 4D printed object can mimic physiological movements, and promote cell growth and differentiation. In this work, we developed an analytical model to predict, in space, the movement of a scaffold that, from a planar geometry, turns into a tubular one. This specific shape change, referred to as "folding", has been chosen because it can mimic several anatomical structures, such as trachea, blood vessels and, in particular, the neural tube, which will be here modelled through human pluripotent stem cells.**

***Keywords*—4D printing, bioprinting, modelling, neural stem cells.**

I. INTRODUCTION

4D printing is a fabrication technique that increases capabilities and application of additive manufacturing (AM) adding time dependent shape changing. In general, a 4D printed structure is defined as a 3D printed structure that changes shape, function and properties because of a predefined external stimulus [1]. Active materials are at the base of 4D printing. They can change their properties in a predefined way after the application of an external stimulus (*e.g.*, variation of moisture, pH, temperature and electromagnetic field). Thus, by combining different materials in a specific spatial distribution it is possible to achieve the desired change of the structure's shape [2]. The control in the spatial arrangement of different materials is achieved with AM, that allows to deposit different materials in a specific pattern with limited constraints [3]. Biomedical related fields of application of 4D printing include: tissue engineering, drug delivery and medical devices. For example, Zareck *et al.* developed a personalized luminal stent using shape memory polymers. More in detail, the device was printed by stereolithography and was capable of increasing its diameter by unfolding once it reaches the site of interest (ideally the patient trachea). Therefore, the final shape of the device is equal to the anatomical site of interest [4]. Another example of 4D printed biomedical application is given by shape memory hydrogels, which have been used to control the target delivery and controlled release of a certain drug after receiving an appropriate stimulus [5]. In the tissue engineering field, 4D printing has been used to produce scaffolds that can influence cell differentiation and growth by shape changing. An example is the study of Hendrikson *et al.* in which they produced a scaffold based on memory shape polyurethane by extrusion based bioprinting, seeded it with human mesenchymal stem cells and demonstrated that scaffold stretching and contraction improved cell activity and adhesion [6]. All these applications are only possible with an appropriate modelling of the shape changing phenomenon. A model is needed to predict the final geometry once the initial shape, material properties and intensity of stimulus are known, due to the several variables that are entangled in the 4D printing process [7]. In this study, an analytical model is developed to predict the shape changing of planar bilayer structures that turn in tubular ones (*i.e.,* self-folding) after immersion in a water solution. More in detail, these structures are homogeneous films of gelatin (fabricated by solvent casting, using an applicator) at high concentration with parallel lines at lower concentration, that were 4D printed on top of the casted gelatin film. Dipping these structures in a water-based solution, the two layers absorb water differently, due to the different gelatin and crosslinker concentrations that determinate a difference of expansion coefficient. This leads to the folding of the structure (Fig.1). The selection of a tubular shape is linked to the evidence that several anatomical parts have a hollow-cylinder like geometry, as examples: blood vessels, nerves and trachea. Additionally, this particular movement is present in the neural tube formation during embryogenesis [8]. The developmental process of neurulation involves a series of coordinated morphological events during embryogenesis, which result in the conversion of the flat neural plate (generated from dorsal ectoderm) into the neural tube, the primordium of the entire central nervous system (CNS) (Fig.1). Failure during neurulation results in neural tube defects, main cause of sever neurodevelopmental pathologies in human [9]. Here, the 4D bioprinted self-folding structure was used to model the neural tube formation, to validate its usability in a biological environment.

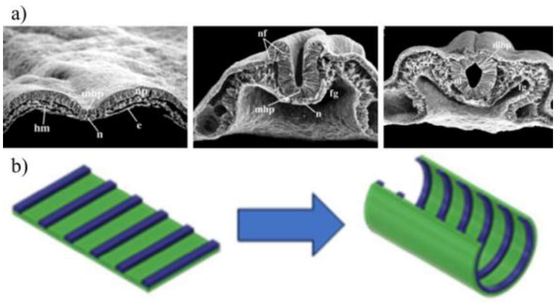

Fig. 1: a) Neurulation process [10] *. b) Folding of produced scaffold*

II. MATERIAL AND METHODS

A. Geometry definition and known models

The geometry to be modelled, can be schematized as a parallelepiped with a series of smaller parallelepipeds on its top (Fig.2).

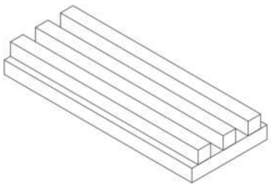

Fig.2: View of modelled geometry

In literature, the most used analysis to predict the bending of a bilayer structure is the Timoshenko's model [11]. In 1925 Timoshenko developed a model that can predict the radius of curvature of a bimetal beam once known the section dimension, mechanical and physical properties of the used materials and the temperature difference. The model is formulated only for beams and in consequence limited to one dimensional (1D) structure. In the next sections, the same steps of Timoshenko's analysis have been applied to the geometry of Fig.1b to obtain the radius of curvature as function of geometric parameters (*e.g.*, moment of inertia of section, thickness of layers, number and dimension of printed lines), material properties (*e.g.,* elastic modulus, expansion coefficient) stimulus intensity (*e.g.*, temperature variation).

B. Hypothesis and simplification

Before starting with model derivation a few assumptions need to be done.

- Since shape morphing happens only where there are two different materials in the film, if parallel lines are thin enough, we can assume that the lines will bend like Timoshenko's beams.
- Zones with only one material will expand but do not contribute to structure folding.
- If the beam width is small enough, the bending angle in this direction can be considered negligible.

With these hypotheses we can assume that the printed lines create a preferential direction for shape change and this direction is the same of the printed ones. In other words, the main axes of the hollow-cylindrical shape will be perpendicular to the printed lines. Moreover, for an easier analysis, expansion coefficients incorporate stimulus intensity. Briefly, instead of expansion coefficient multiplied by the stimulus intensity, we consider directly the resulting strain. This is justified by the use of moisture as trigger, because moisture intensity is always the same in water solutions.

C. Model derivation

The following material and geometrical properties are known: Young's modules (E_1 and E_2), expansion coefficients along L direction ($\alpha_1$par, $\alpha_2$par), expansion coefficients along h direction ($\alpha_1$per, $\alpha_2$per), thickness of homogeneous film and printed lines (h_1, h_2), width of lines (D), width of homogeneous film (W) (Fig.3). Hypotheses are verified if D is negligible compared to W and to total length (L). Therefore, without external forces we can consider only internal forces (P) and torques (m) acting along the direction parallel to lines. All geometrical parameters and acting forces are shown in Fig.3.

Since no external forces are present, internal forces and torques are in equilibrium (Eq.1 and Eq.2):

$$P_1{}' + P_1{}'' = P_2 = P \quad (1)$$

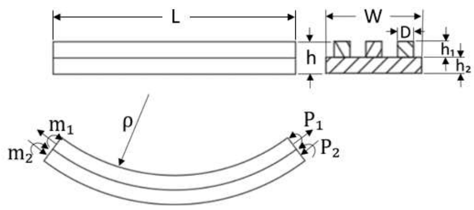

Fig.3: Geometrical parameter and acting force on the structure, before and after shape change.

$$P * \frac{h}{2} = m_1{}' + m_1{}'' + m_2 \quad (2)$$

In the Eq.1 and Eq.2 only two lines of material 1 are considered. More in general, since we have N printed lines, total force and momentum in the lines is the sum of forces and momentum in each line (Eq.3 and Eq.4):

$$\sum_1^N P_{1i} = P_2 = P \quad (3)$$

$$P * \frac{h}{2} = \sum_1^N m_{1i} + m_2 \quad (4)$$

If we consider that printed lines have all same size and are equally spaced, then also lines internal forces and torques are all equal ($P_1 i = P_1 \; and \; m_1 i = m_1$), and Eq.3 and Eq.4 become Eq.5 and Eq.6, respectively.

$$N * P_1 = P_2 = P \; (5)$$

$$P * \frac{h}{2} = N m_1 + m_2 \quad (6)$$

Defining ρ as radius of curvature of the structure, torques are obtained from Eq.7, where $I_1 = \frac{D*h_1{}^3}{12} \; and \; I_2 = \frac{W*h_2{}^3}{12}$.

$$m_1 = \frac{E_1*I_1}{\rho} \qquad m2 = \frac{E_2*I_2}{\rho} \, (7)$$

Substituting Eq.7 in Eq.6 we obtain Eq.8:

$$P * \frac{h}{2} = \frac{N*E_1*I_1 + E_2*I_2}{\rho} \quad (8)$$

The sheared surface between the two materials (parallel direction) the strains of the two materials must be equal (Eq.9):

$$\alpha_1 + \frac{P_1}{E_1*h_1*D*N} + \frac{h_1}{2*\rho} = \alpha_2 - \frac{P_2}{E_2*h_2*W} - \frac{h_2}{2*\rho} \; (9)$$

In Eq. 9 the first terms $\alpha 1$ and $\alpha 2$ are deformations caused by material expansion, second terms are strain calculated according to Hooke model and third terms describe the folding from Navier's Equation.
Substituting Eq.8 in Eq.9 we obtain Eq.10:

$$\frac{1}{\rho} = \frac{(\alpha_2 par - \alpha_1 par)}{\frac{h}{2} + \frac{2*(N*E_1*I_1 + E_2*I_2)}{h} * \left(\frac{1}{E_1*h_1*N*D} + \frac{1}{E_2*h_2*W}\right)} \; (10)$$

Defining $m = h_1/h_2$, $n = E_1/E_2$ and $\beta = ND/W$, Eq.10 can be written as Eq.11:

$$\frac{1}{\rho} = \frac{6(\alpha_2 par - \alpha_1 par)(m+1)^2}{h(3(m+1)^2 + (1+\beta mn)(m^2 + 1/\beta mn))} \quad (11)$$

The radius of curvature results proportional to the total thickness and inversely proportional to the difference in elongation of the two materials. The other parameters m, n and β influence the value of ρ but in a not trivial way.

D. *Model validation*

To validate this analytical model we produced samples with the same geometry described in section IIA.

These structures were made by a homogeneous film produced by solvent casting using an applicator, thus guaranteeing a homogeneous thickness, composed by a 15% w/v type A gelatin from porcine skin in PBS solution 1X with the addition of 92µl of γ-glycidoxypropyltrimethoxysilane (GPTMS) for each gram of gelatin. On top of the film equidistant parallel lines were printed by extrusion-based bioprinting. Those lines consist of a 5% w/v type A gelatin from porcine skin in PBS solution 1X with 368µl of GPTMS for each gram of gelatin (Fig.4a).

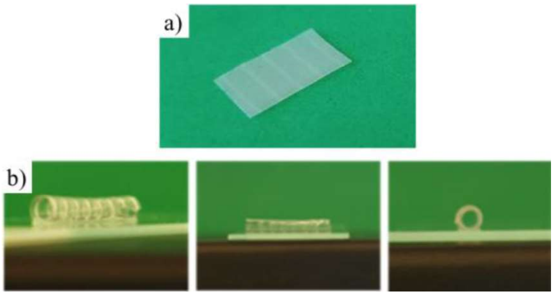

Fig. 4: Scaffold produced of dimension 10x5mm, a) before actuation, b) after folding

The material was chosen for its biocompatibility [12], and the solutions concentrations were chosen to maximise the difference of swelling ratio between the two materials (data not shown). Since the two layers are made by the same bulk materials a chemical bound occur between the two layers. This phenomenon eliminates the risk of delamination of the structure. Both materials have been physically and mechanically characterized to determinate elastic modulus (under wet and dry conditions) and expansion coefficients ($\alpha = \frac{final\ length - initial\ length}{initial\ length}$). The results of these characterization are shown in Table I.

TABLE I: MECHANICAL AND PHYSICAL PROPRIETIES

Material	E wet (MPa)	E dry (MPa)	αpar (%)	αper (%)
Gelatin 15%	3.81 ± 0.43	3170 ± 280	8.54±1.35	164.70±8.67
Gelatin 5%	63.13 ± 26.72	1820 ± 550	3.14± 1.89	38.67±16.52

Values are written as mean ± standard deviation, 4 samples are used to estimate E and 10 samples are used to estimate α

Validation of the model is based on comparing the model predicted radius of curvature (mean and standard deviation STD of the model derived from estimated variability of physical/mechanical properties) of the structure and the effective radius of curvature measured on the real samples, as function of one or more parameters. The thickness of the homogeneous film is the parameter that, from Timoshenko's model, gives larger variation of the radius of curvature. For this reason, the radius of curvature was measured for different h2 values and compared to the predicted ones.

Fabricated samples are 10x5mm on plane and have a total thickness varying from 50µm to 160µm. Layers thickness was measured with a micrometer (h_1, h_2 and h), while lengths on the plane was measured from hi-res figures using the software ImageJ (D and W). Results of measurement are shown in Table II. To trigger the shape changing of the structures the samples were dipped in PBS 1X and after 3 hours (time needed to reach the plateau of expansion, determined during the measure of the expansion coefficient, data not shown) the radius of curvature was measured from pictures using ImageJ.

TABLE II: GEOMETRICAL PARAMETERS

h2 (µm)	h1 (µm)	D (mm)	W (mm)
50-160±5	33.1 ± 14.1	1.0±0.1	10.2±0.4

Values are written as mean ± standard deviation, 30 samples are used to obtain h1, D and W measures

E. *Biological application*

Scaffolds used to validate the model have been also used to explore the effects of 4D bioprinting in cell differentiation and growth. More in detail, *in vitro* modelling of neural tube formation was explored. A customized holder was put on the scaffold while it was still flat in water-based solution to kept the scaffold flat. The operator just needed to remove the holder to actuate the folding movement. Holder was needed to give time to cell to attach on the scaffold, otherwise shape changing would start too early and the cells would not follow the scaffold movement.

Human induced pluripotent stem cells (hiPSCs) were seeded on 4D bioprinted scaffolds and on 2D static films. After 24 hours, 4D scaffolds were actuated and 3 days later, when the cells reached > 90% confluence, neural induction protocol [13] started. After 12 days of neural induction, cells were driven to differentiation for 4 days, by adding neural differentiation supplemented with the neurotrophin BDNF. Neural differentiation was evaluated through immunofluorescence assay. Confocal imaging of immunoassayed 4D scaffold revealed homogeneous positivity for Nestin [14] (intermediate filament protein of neural progenitors) and SOX2 [15] (transcription factor expressed in neural progenitors), thus confirming successful neural identity.

III. RESULTS

A. *Predicted and measured radius comparison*

Radius of curvature values are plotted as function of the total thickness as shown in Fig.5.

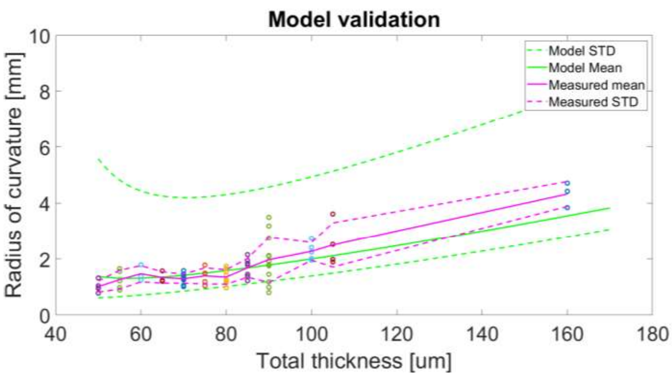

Fig.5: Predicted and measured radius in function of the total thickness. Each dot is a sample.

Mean values of the model (continuous green line) are calculated using mean value of measured material and geometrical parameters (*i.e.*, Young's modulus, expansion coefficients, film thickness, lines thickness and width) STD values of the model (dotted green lines) are calculated using upper and lower values of material and geometrical parameters. For each thickness and radius measure a dot is plotted, obtaining mean (continuous magenta line) and STD (dotted magenta lines). Predicted and experimental values fall in the same region, when the total thickness of the 4D printed structure is between 55 and 105µm.

B. *Biological application*

Cells attached to the scaffold within 24h after seeding (Fig.6a, top panels). After holder removal, cells still adhere to scaffold surface and within 48h colonize the whole scaffold surface (Fig.6a, bottom panels). Morphological changes occurring during neural induction phase suggest neural commitment (Fig.6b).

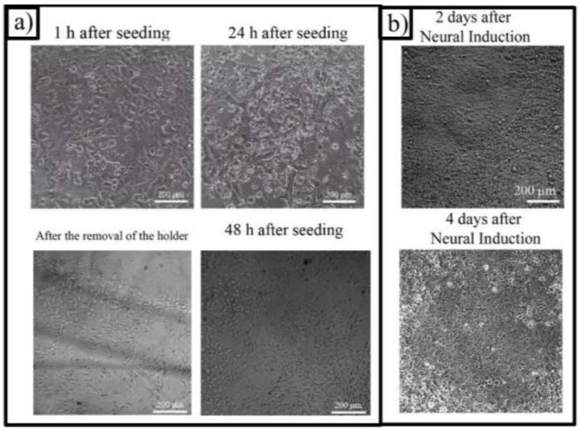

Fig. 6: a) Cells attachment after seeding b) Cells are homogeneously distributed on scaffold surface during neural induction showing morphological change due to neural commitment

After 12 days of neural induction, cells extensively express Nestin and SOX2 neural progenitor typical markers (Fig.7a) and organize into neural rosettes (Fig.7a, bottom panel). Moreover, after 4 days of differentiation, cells seem to be oriented along the thickness of the scaffold, showing a similar organization of neural progenitors in the native neural tube (Fig.7b).

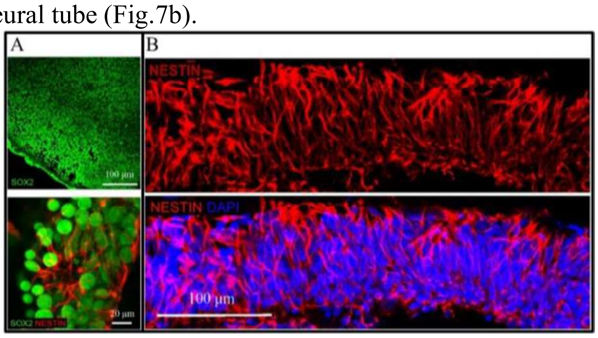

Fig.7: Representative confocal analysis showing A) neuroepithelial-like structure expressing Nestin and SOX2 (DIV12) B) maintenance of the apical-basal orientation of neural precursor at DIV16

IV. Conclusion

The developed model can be used to design self-folding scaffolds that can have multiple purposes in tissue engineering. The model allows to completely control bending orientation and predict the curvature radius of the scaffolds, and to achieve self-folding scaffolds with customizable length, diameter and degree of curvature as a result. Looking at the mathematical model itself, it needs to be improved by adding the time dependent behaviour. In this way, we can achieve a model capable to predict the change in shape through space and time.

The 4D printed scaffold was then used to develop a neural tube in vitro model. Indeed, the self-folding movement of the scaffold recapitulate the formation of neural tube in vitro. The scaffold resulted to be highly biocompatible. Moreover, shape change seems to sustain neural differentiation as showed by immunofluorescence assay with diagnostic markers. Neural tube experiment showed the differentiation from pluripotent cells (hiPSCs) to patterned neural progenitor cells, as highlighted by the expression of Nestin and SOX2. An exhaustive gene characterization in longer period of differentiation is ongoing, to evaluate if 4D printed scaffolds can support neural progenitor differentiation into mature neurons.

Acknowledgement

This study received funding from the European Union Next-Generation – National Recovery and Resilience Plan (NRRP) – MISSION 4 COMPONENT 2, INVESTMENT ECS00000017 - Tuscany Health Ecosystem, CUP N. 153C22000780001 (Spoke4: Nanotechnologies for diagnosis and therapy and Spoke8: Biotechnologies and imaging in neuroscience). This manuscript reflects only the authors' view and options, neither the European Union nor the European Commission can be considered responsible for them.

References

[1] J. Choi, O. C. Kwon, W. Jo, H. J. Lee, and M. W. Moon, "4D printing technology: A review," *3D Printing and Additive Manufacturing*, vol. 2, no. 4. Mary Ann Liebert Inc., pp. 159–167, Dec. 01, 2015

[2] Q. Ge, C. K. Dunn, H. J. Qi, and M. L. Dunn, "Active origami by 4D printing," *Smart Mater Struct*, vol. 23, no. 9, 2014

[3] A. Sydney Gladman, E. A. Matsumoto, R. G. Nuzzo, L. Mahadevan, and J. A. Lewis, "Biomimetic 4D printing," *Nat Mater*, vol. 15, no. 4, pp. 413–418, Apr. 2016

[4] M. Zarek, N. Mansour, S. Shapira, and D. Cohn, "4D Printing of Shape Memory-Based Personalized Endoluminal Medical Devices," *Macromol Rapid Commun*, vol. 38, no. 2, Jan. 2017

[5] Y. Wang *et al.*, "Three-dimensional printing of shape memory hydrogels with internal structure for drug delivery," *Materials Science and Engineering C*, vol. 84, pp. 44–51, Mar. 2018

[6] W. J. Hendrikson, J. Rouwkema, F. Clementi, C. A. van Blitterswijk, S. Farè, and L. Moroni, "Towards 4D printed scaffolds for tissue engineering: Exploiting 3D shape memory polymers to deliver time-controlled stimulus on cultured cells," *Biofabrication*, vol. 9, no. 3, Aug. 2017

[7] F. Momeni, S. M.Mehdi Hassani.N, X. Liu, and J. Ni, "A review of 4D printing," *Mater Des*, vol. 122, pp. 42–79, May 2017.

[8] N. D. E. Greene and A. J. Copp, "Development of the vertebrate central nervous system: Formation of the neural tube," *Prenatal Diagnosis*, vol. 29, no. 4. pp. 303–311, Apr. 2009

[9] C. Dell' Amico, A. Tata, E. Pellegrino, M. Onorati, and L. Conti, "Genome editing in stem cells for genetic neurodisorders," *Prog Mol Biol Transl Sci*, vol. 182, pp. 403–438, Jan. 2021

[10] J. Ois Colas and G. C. Schoenwolf, "Towards a Cellular and Molecular Understanding of Neurulation," 2001.

[11] S. Timoshenko, "Analysis of bi-metal thermostat," *Josa*, 11.3:233-255, Sept. 1925.

[12] A. Lapomarda *et al.*, "Pectin as rheology modifier of a gelatin-based biomaterial ink," *Materials*, vol. 14, no. 11, Jun. 2021

[13] L. Conti and E. Cattaneo, "Neural stem cell systems: Physiological players or in vitro entities?," *Nature Reviews Neuroscience*, vol. 11, no. 3. pp. 176–187, Mar. 2010.

[14] Gilyarov, A. V. "Nestin in central nervous system cells." *Neuroscience and behavioral physiology* 38.2: 165-169. 2008

[15] L. H. Pevny and S. K. Nicolis, "Sox2 roles in neural stem cells," *International Journal of Biochemistry and Cell Biology*, vol. 42, no. 3. pp. 421–424, Mar. 2010